Fractionation by Spatially Heterogeneous Diffusion: Experiments and Two-Component Random Walk Model

Hoyoun Kim[†,§,#], KeunMin Ken Lee[‡,#], Gadisa Firisa[‡], Juncheol Lee[‡], Myung Chul Choi*[,‡] and Yong-Jung Kim*[,†]

[†]Department of Mathematical Science, Korea Advanced Institute of Science and Technology (KAIST), Daejeon 34141, Republic of Korea

[‡]Department of Bio and Brain Engineering, Korea Advanced Institute of Science and Technology (KAIST), Daejeon 34141, Republic of Korea

[§]Computer, Electrical and Mathematical Sciences and Engineering Division (CEMSE), King Abdullah University of Science and Technology (KAUST); Thuwal, 23955, the Kingdom of Saudi Arabia.

[#]These authors contributed equally to this work

E-mail: mcchoi@kaist.ac.kr, yongkim@kaist.ac.kr

ABSTRACT

The fundamental question regarding the fractionation phenomenon is whether diffusion alone is responsible for it or if an additional advection dynamic is involved. We studied the fractionation by diffusion of particles in spatially heterogeneous environments. By experimentally observing the time-sequential fractionation patterns of dye particles diffusing across a solid-solid interface of varying polyacrylamide gel densities, we found that the *two-component diffusion model* accurately captures the observed fractionation dynamics. In contrast, single-component diffusion models by Fick, Wereide, and Chapman do not. Our results indicate that diffusion alone can explain the fractionation phenomenon and that additional advection dynamics are not involved. The underlying physics in the fractionation phenomenon is discussed using a *two-component random walk model*.

INTRODUCTION

Diffusion, a macroscopic phenomenon driven by the random microscopic movement of particles, is well-understood in homogeneous environments. In 1855, Fick introduced the concept of diffusion flux, $J_F = -D\nabla u$, where ∇u is the gradient of the particle concentration in water, and D is the diffusivity constant. This diffusion law states that particles move from regions of high concentration to low concentration, leading to an eventual homogenization of their distribution. Fifty years later, Einstein further elucidated this process using a random walk model and linked Fick's concept of homogeneous diffusion to molecular-level physics[1].

In 1856, one year after Fick's paper, Ludwig[2] observed that salt particles move toward higher concentration regions if temperature T is spatially non-constant. Soret[3] confirmed this fractionation phenomenon and experimentally showed that this uphill diffusion appears when the temperature is not uniform. Since then, numerous examples of the Ludwig-Soret effect in liquids and gases have been observed[4–9], which led to the development of thermal diffusion equations that include thermal advection terms.

The phenomenon of fractionation is not limited to fluid phases. Dominguez[10] studied isotope fractionation via thermal gradient in silicate melts subject to high temperatures. On the other hand, Darken[11] showed that, even if the temperature is homogeneous, the fractionation of carbon appears in an austenite rod when its composition is discontinuous along a solid-solid interface[12,13]. He replaced the thermal advection term with the chemical-potential 'advection term' introduced by Nernst[14]. Milligen *et al.*[15] observed the fractionation of dye particles in a liquid-solid interface, where green food dye particles diffuse towards gelatin.

Furthermore, fractionation phenomena have been gaining interest, especially in biological systems, where selective fractionation of particles, such as proteins and nanoparticles, plays an important role in cellular functions. Specifically, the passive nature of processes observed in liquid-liquid phase separation[16–18] and perinuclear accumulation of functional particles[19–22] offers an alternative transport mechanism within living organisms that is energy-efficient and incurs no energy cost.

The theoretical explanations for the Ludwig-Soret effect were contributed by Chapman[23–26], Enskog[27], Wereide[28], and Onsager[29], though their studies were focused primarily on thermo-diffusion in gaseous mixtures. In particular, Chapman developed his diffusion model to explain the fractionation phenomenon using diffusion alone. However, differing opinions on the physical cause of the Ludwig-Soret effect in liquid have emerged, with proposals ranging from activation self-diffusion free enthalpies[30] to solvation entropy[31]. Researchers today often use diffusion models supplemented with various advection terms tailored to each system, yet in many cases, the physical evidence for these advection terms remains elusive.

Consequently, there has been much debate about which diffusion law is correct when diffusivity varies spatially. Some claim no universal form of diffusion equation exists[32,33], while others argue that diffusion law is only a convention as long as the added advection term is suitable[34,35]. The remaining key question about the fractionation phenomenon is whether diffusion alone is responsible for it or if an additional advection dynamic is involved. This controversy stems from two facts. First, due to the nature of the diffusion phenomenon, it is hard to experimentally obtain time-sequential dynamics data with the accuracy needed to verify diffusion laws, which consequently makes it difficult to determine whether a diffusion model aligns with the phenomenon or if an additional advection dynamic is present. Second, diffusivity alone cannot explain heterogeneous diffusion phenomena, as all attempts so far have used a single diffusion coefficient D to explain the fractionation phenomenon.

In this paper, we present for the first time the time-sequential dynamics data, and we demonstrate that two-component diffusion law alone can explain the fractionation phenomenon exactly. More specifically, Kim *et al*. derived two-component diffusion model[36–40] extending Einstein's random walk idea after adding spatial heterogeneity. The model divides the diffusivity into two parts, $D = KM$, and the diffusion flux is written as

$$J_{\mathrm{K}} = -K(x)\,\nabla(M(x)u), \qquad D(x) = K(x)M(x). \tag{1}$$

When M is constant, Eq. (1) reduces to Fick's law. If we consider two-component random walk model and denote the walk length of diffusing particles by $l(x)$ and the sojourn time by $\tau(x)$, the diffusion flux in Eq. (1) becomes

$$J_{\mathrm{K}} = -\frac{l(x)}{2n}\,\nabla\left(\frac{l(x)}{\tau(x)}u\right), \qquad D(x) = \frac{l^2(x)}{n\tau(x)}, \tag{2}$$

where n is the space dimension. We find that the experimentally measured coefficient values closely match the estimates obtained from comparing lattice systems with different acrylamide densities.

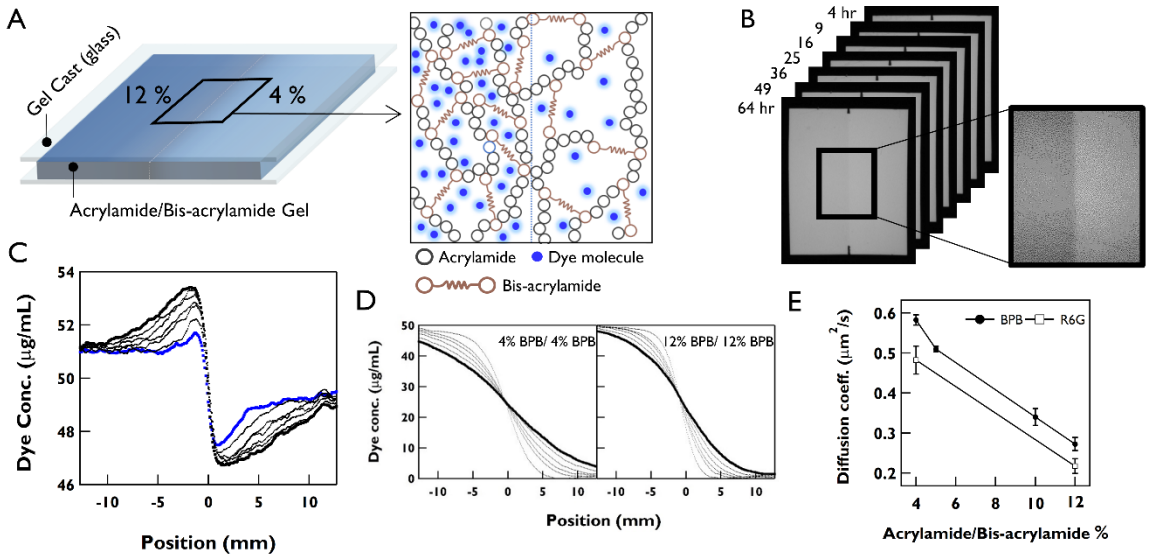

Fig. 1 Fractionation at spatially heterogeneous gel interfaces. (A) Schematic view of the experimental setup, depicting two adjoining polyacrylamide gels with different acrylamide/bis-acrylamide concentration and the transition layer. (B) Snapshots of the experiment taken between 4 to 64 hours. The 64 hr snapshot, magnified on the right, is contrast-adjusted to highlight fractionation. (C) Dye concentration between 4 hours (blue dots) and 64 hours (thick black dots) for $_{BPB}G_{12\%,4\%}$. The initial distribution at 4 hours forms as the gel interface fully polymerizes. (D) Dye concentration profiles for homogeneous cases with gel densities of 4% (left) or 12% (right). Gel at $x > 0$ initially contains no dye. (E) The diffusivities for the four gel densities and two dye types, BPB (circle) and R6G (square).

RESULTS AND DISCUSSION

Fractionation at spatially heterogeneous gel interfaces.

We observed dynamic fractionation patterns of dye concentration diffusing across a spatially heterogeneous solid-solid interface (Fig. 1A). This interface was made by adjoining two gels made of water and acrylamide/bis-acrylamide (or simply acrylamide) solution (see Methods: Polyacrylamide gels with heterogeneous lattice interface). Selected for their clarity, structural stability when hydrated, and adjustable pore size, these gels allow precise observation of dye movement across a solid-solid interface that provides spatial heterogeneity. Specifically, we manipulated the lattice size (or porosity) by varying the acrylamide concentration of the gel and pouring it over an already solidified one (Fig. 1A magnified inset). Consequently, the pore size of our polyacrylamide gels ranged from approximately 70 to 130 nm[41]. The dye particles we used for the experiments were Bromophenol Blue (BPB) and Rhodamine 6G (R6G) selected for their small particle size of 2–3 nm and long-lasting color fastness, making them ideal for extended observation periods.

Four experimental groups, each representing different gel density combinations and dye types, are used. For example, in the $_{BPB}G_{12\%,4\%}$ group, one side of the interface is a gel with 4% acrylamide, and the other with 12%. Similar setups were used for $_{R6G}G_{12\%,4\%}$, $_{BPB}G_{10\%,5\%}$, and $_{BPB}G_{5\%,10\%}$. In each case, the higher percentage gel was injected later to minimize the transition time, except for $_{BPB}G_{5\%,10\%}$.

We measured the absorbance of BPB or R6G eight times at intervals of k^2 hours, where k = 1, 2, …, 8 (Fig. 1B). The 1-hour snapshot was excluded because the solidification process of the second gel

occurred during the first hour. To mitigate boundary effects, only the central part of each snapshot was taken (see Methods: Data Extraction Process). The absorbance data were converted to one-dimensional dye concentration profiles. This time-sequential image shows the fractionation dynamics over time (Fig. 1C, see Methods: Dye standard curve measurement). Since the 4-hour snapshot (in blue, Fig. 1C) is taken 4 hours after the second gel is injected, the diffusion process has already begun, resulting in a step-like distribution.

Fig. 1D shows how we measured the diffusivity of each gel concentration. The second half of the gel cast was filled with the same concentration gel without dye particles, and then the diffusion of dye particles was measured. The two images in Fig. 1D are the processed data for the two homogeneous cases. Diffusivities for the four gel densities and two dye types used in the experiment were obtained from multiple runs of experiments and are given in Fig. 1E. The average diffusivities measured are $D_{12\%} = 0.2725$ mm^2/hr for BPB in 12% acrylamide gel and $D_{4\%} = 0.5825$ mm^2/hr for BPB in 4% gel. The heterogeneous diffusivity $D(x)$ for ${}_{\mathrm{BPB}}G_{12\%,4\%}$ takes these values for $x < 0$ and $x > 0$, respectively.

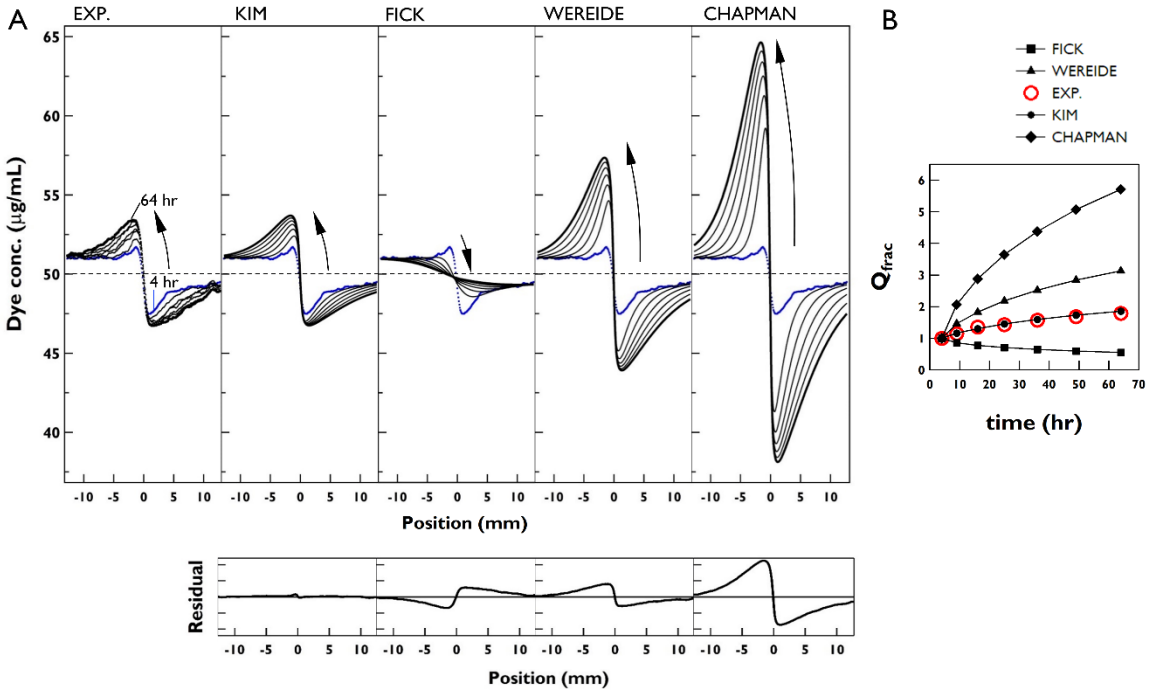

Fig. 2 Comparisons of fractionation with four diffusion models. (A) Comparison of ${}_{\mathrm{BPB}}G_{12\%,4\%}$ experimental result with four diffusion model predictions. The initial dye distribution is represented in blue, with time-sequential fractionation patterns (black) are shown with the final fractionation emphasized. The residual at 64 hours is displayed below each model's prediction. (B) Quantitative comparison of fractionation quotient Q_{frac} values. Experimental data (red circle) are compared with Fick (square), Wereide (triangle), Chapman (diamond) and Kim (circle).

Comparison of fractionation with four diffusion models.

The experimental data from ${}_{\mathrm{BPB}}G_{12\%,4\%}$ group and the numerical estimates from four diffusion models are compared in Fig. 2. The diffusion fluxes for these models are given by: Fick's model ($J_F = -D\nabla u$), Wereide's[28] model ($J_W = -\sqrt{D}\,\nabla(\sqrt{D}u)$), and Chapman's[23,42] model ($J_C = -\nabla(Du)$). Since these three

diffusion fluxes depend solely on the diffusivity D, we call them single-component models. In contrast, Kim's two-component diffusion flux J_K in (1) requires two coefficients, K and M.

The numerical estimates given in Fig. 2A are solutions of a differential equation, $\partial_t u = -\partial_x J$, with the initial condition $u(4, x) = u_4(x)$, where $u_4(x)$ is the experimental data at 4 hr (blue dots) and J is one of the four diffusion fluxes. In Fig. 2A, experimental data are compared with numerical estimates. Fick gives homogenization, showing flattening of dye concentration pattern over time, while Chapman and Wereide give too much fractionation. To use Kim's two-component diffusion flux, we need one more coefficient. Roughly speaking, we took $M(x) = M_-$ for $x < 0$ and set $M(x) = M_+$ for $x > 0$. Since J_K is invariant for constant multiplication of $K(x)$ and $M(x)$ as $J_K = -K(x)\nabla(M(x)u) = -CK(x)\nabla\left(\frac{M(x)}{C}u\right)$, we can choose $M_- = 1$ without loss of generality (i.e. choosing $C = M_-$). Then, $K(x)$ is simply given by $K(x) = D(x)/M(x)$. The next step is to find M_+ that fits the data best using the least square method. Therefore, it is not surprising that the two-component diffusion model gives the best fit in Fig. 2. The surprising finding is that the fit is near perfect (Fig. 2A bottom) that this result tells us that no additional convection dynamics exist; the two-parameter diffusion model alone is sufficient. The fractionation quotient Q_{frac} is given in Fig. 2B to quantify the fractionation degree, which measures the difference in dye amounts between two sides, normalized by the net dye amount (see Methods: Q_{frac} calculation for the definition of Q_{frac}).

Physics and Mathematics behind fractionation.

The two-component diffusion flux J_K disappears when Mu is constant, meaning that u becomes inversely proportional to $M(x)$ at equilibrium. To see the physical meaning of $M(x)$, we need to see the connection between $M(x)$ and random walk parameters. The lattice model appears to be the best fit for describing the diffusion phenomenon across acrylamide gels. Suppose that a particle jumps the walk-length $\Delta x = l(x)$ every sojourn time $\Delta t = \tau(x)$. Then, coefficient M is given by $M(x) = l(x)/\tau(x)$ (see SI: Derivation of two-component diffusion flux). Therefore, at the equilibrium state, $J_K = 0$ gives $l(x)u/\tau(x) =$ constant, meaning the particle density (or concentration) u is proportional to $\tau(x)$ and inversely proportional to $l(x)$. This aligns with the physical intuition that equilibrium is obtained when the particle mass flux across heterogeneous gel interface is balanced. At the heterogeneous interface $x = 0$, the mass flux for $x > 0$ is written as $J_+ = \rho N_+/(2nA_+\tau_+)$, where ρ is molar mass, N_+ is the number of particles inside a lattice for $x > 0$, A_+ is the area of one side of the lattice, and τ_+ is sojourn time. Here, the term $2n$ is because of the number of faces on n-dimensional lattice. Since the mass density is defined as $u_+ = \rho N_+/V_+$, we can rewrite the flux as $J_+ = l_+u_+/(2n\tau_+)$. At the equilibrium, this flux should be balanced with the flux from negative domain, $J_+ = J_-$. Thus, the relation $M(x)u =$ constant is obtained again where coefficient M is given by $M(x) = l(x)/\tau(x)$. However, $l(x)$ and $\tau(x)$ do not necessarily change linearly. In other words, M_+ and M_- can differ. This leads to fractionation over time because they should satisfy $u_+/u_- = M_-/M_+$ at the equilibrium.

To measure the fractionation quantitatively, we use the exponent q of diffusivity as $M_-/M_+ = (D_-/D_+)^q$. In heterogeneous environment, if $D \neq 1$, we can express $M(x) = D^q(x)$ where $q(x) = \ln M(x)/\ln D(x)$ (see SI: Derivation of exponent form of diffusion flux), and hence the flux J_K is written as $J_q = -D^{(1-q)}\nabla(D^q u)$. In this notation, we denote only the variation in $K(x)$ and $M(x)$ using $D(x)$. Using this form has an advantage: the three one-component diffusion fluxes are in this form, where $J_F = J_0$, $J_W = J_{0.5}$, and $J_C = J_1$. For the two-component diffusion law, the exponent q varies in space, i.e., $J_K = J_{q(x)}$. In our experiment, since the diffusivity is constant for $x < 0$ and $x > 0$, we can choose a constant q as $q = \ln(M_+/M_-)/\ln(D_+/D_-)$ when $D_+ \neq D_-$. If the gel concentration or the dye particle types are changed, the corresponding exponent q changes depending on the change of M compared to D. In a previous discussion, we fixed $M_- = 1$ and used M_+ as a fitting parameter. Equivalently, we can take the

exponent q as a fitting parameter since D_+ and D_- can be measured independently (see Methods: Numerical estimations for heterogeneous diffusion). This approach allows us to compare the two-component flux to single-component ones.

From Eq. (2), we see that if $\tau(x)$ is constant and $l(x)$ varies, the exponent corresponding to the flux J_K is $q = 0.5$. If $l(x)$ is constant and $\tau(x)$ varies, then $q = 1$. If $\tau(x)$ is proportional to $l(x)$, then the ratio $l(x)/\tau(x)$ is constant and hence $q = 0$. We are analyzing our experiment using a lattice model where we assume dye particles jump instantly from one lattice to another every sojourn time. Assuming no other interactions (such as attraction or repulsion) are present, as the lattice size grows, the dye particles' walk length will increase. Simultaneously, because the lattice cell is now larger, it would take longer for dye particle to jump to the next cell. Therefore, we expect that $q < 0.5$ in our experiment. Since we observed the fractionation across the heterogeneous interface, the rate of change should be different; otherwise, $\tau(x)$ would be proportional to $l(x)$ resulting in no fractionation as the system will follow Fick's law. Additionally, if $\tau(x)$ were to increase faster than $l(x)$, resulting q would become negative which means larger dye density with higher diffusivity. This inverse fractionation is mathematically possible, but its existence in physical system is questionable as it is counter intuitive. Therefore, we expect $\tau(x)$ to increase as $l(x)$ increase, but at a slower rate than $l(x)$, leading to $q > 0$. In fact, we find the exponent corresponding to the experiment in Fig. 2 is $q = 0.254$.

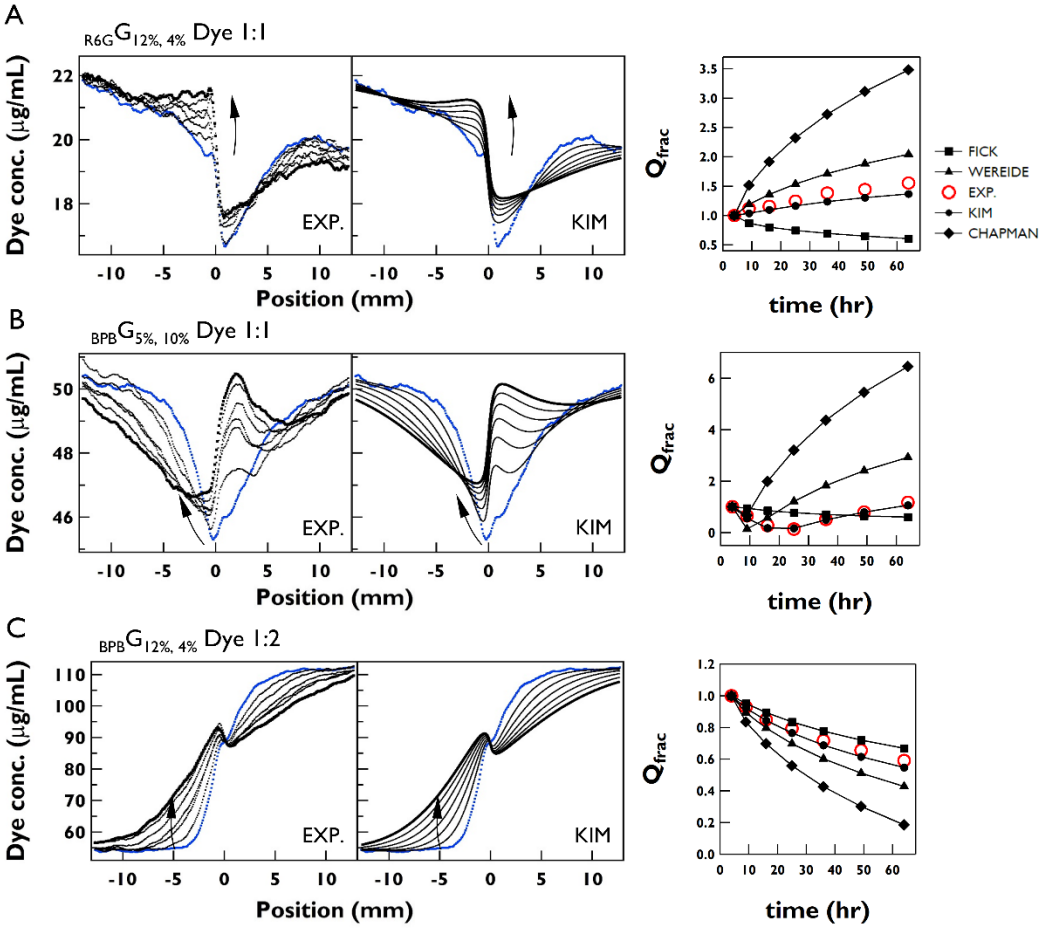

Fig. 3 Dye type, gel density, and initial distribution effect in fractionation. Comparison of dye distribution in the $_{R6G}G_{12\%,4\%}$ (A), $_{BPB}G_{5\%,10\%}$ (B) and $_{BPB}G_{12\%,4\%}$ (C) experiments and corresponding numerical estimates from 4 hours (blue) up to 64 hours (black, 64 hr highlighted). On the right, Q_{frac} for each hour are compared between experiment (red circle), Fick (square), Wereide (triangle), Chapman (diamond) and Kim (circle).

Effects of dye type, gel density, and initial distribution.
We investigated the fractionation dynamics for three more cases by varying dye type, gel density, and initial distribution. In Fig. 3A, time-sequential experimental patterns from the $_{R6G}G_{12\%,4\%}$ group are shown alongside a numerical estimate using the two-component model. The corresponding *q*-value of the group is $q = 0.267 \pm 0.042$, which is slightly bigger than the case of Fig. 2. The size of R6G based on its chemical structure is slightly larger (~1 nm) than that of BPB, which affects the fractionation process and changes the *q*-value. The distribution pattern evolves to a step function-like equilibrium state and it is well captured by the two-component (see Fig. S1A for the performance of other single-component models). In Fig. 3B, an example from the $_{BPB}G_{5\%,10\%}$ group is given, which gives $q = 0.236 \pm 0.017$. For this case, the higher density gel (10%) was solidified first in $x > 0$, followed by the lower density gel (5%). Because the 5% gel takes longer to solidify than 10% gel, the initial profile at $t = 4$ hr is significantly different from other cases. The two-component model still accurately predicts the pattern and the Q_{frac} value (Fig. S1B). Compared to the result for the $_{BPB}G_{12\%,4\%}$ case in Fig. 2, *q*-value is decreased, and the change is greater than the $_{R6G}G_{12\%,4\%}$ case, meaning the lattice size has greater impact on fractionation than the dye size. In addition, the initial amount of dye was doubled in the 4% gel region ($x > 0$) of the $_{BPB}G_{12\%,4\%}$ case in Fig. 3C. The corresponding *q*-value of the group is $q = 0.254 \pm 0.044$. Due to the additional dye, the initial distribution appears fractioned in the opposite direction. However, the diffusion process reverses this pattern starting from the interface, eventually leading to a result consistent with the previous outcomes. The two-component diffusion model accurately generates this reversal (Fig. S1C).

The two-component diffusion flux is given by the two coefficients $K(x)$ and $M(x)$, and the numerical estimates using this two-component model were confirmed to be in perfect agreement with the experimental classification pattern for three more cases. These findings serve as evidence that the fractionation phenomenon is driven solely by diffusion.

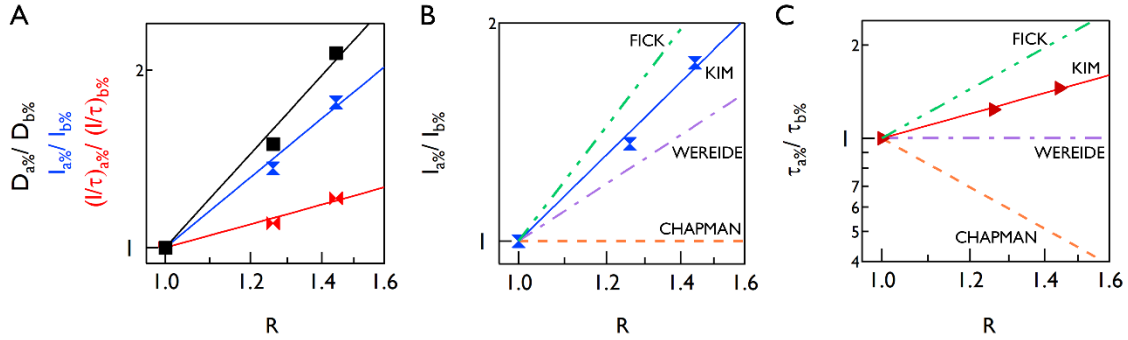

Fig. 4 Lattice size effect on random walk parameters. (A) The plot comparing the experimental ratios of diffusivity *D* (black), *l* (blue) and l/τ (red) against the lattice size ratio R in log-log scale. The power law relationships between these ratios and R are depicted, with exponents being 1.9835 ± 0.102 for *D*, 1.4899 ± 0.0664 for *l*, and 0.49598 ± 0.0364 for l/τ. Note when *l* and l/τ are multiplied, we recover the exponent value for *D* ratio as expected. (B) Comparison of the experimental *l* ratio (blue) vs. R with theoretical prediction by Kim (blue), Fick (green), Wereide (purple) and Chapman (orange), log-log scale. (C) Comparison of the

experimental τ ratio (red) vs. R with Kim (red), Fick (green), Wereide (purple) and Chapman (orange) models (log-log scale).

Two-component random walk and lattice size effect.

Since the fractionation depends on the ratio of M across the interface, the following analysis is given in terms of such ratios. We take a lattice model for this analysis. Let L be the average edge length of lattice composed of the acrylamide gel. Since the length L is inversely proportional to the cube root of the gel density, for the ${}_{BPB}G_{12\%,4\%}$ group, the ratio of the two length sizes in three dimensions is, $R_{12\%,4\%} = L_{4\%}/L_{12\%} = \sqrt[3]{12/4} = 1.442$. Similarly, $R_{10\%,5\%} = 1.26$. The experimentally obtained ratios for $D_{a\%}/D_{b\%}$, $l_{a\%}/l_{b\%}$ and $(l/\tau)_{a\%}/(l/\tau)_{b\%}$ for the two groups with respect to R is plotted in Fig. 4A. In the two-component model, $D_{a\%}/D_{b\%}$ is shown to be in $\sim R^2$ relationship, $l_{a\%}/l_{b\%} \sim R^{3/2}$ and $(l/\tau)_{a\%}/(l/\tau)_{b\%} \sim R^{1/2}$. We can use the last two relationships to obtain $\tau_{a\%}/\tau_{b\%} \sim R$ shown in Fig. 4C.

In detail, for the ${}_{BPB}G_{12\%,4\%}$ group, $l_{4\%}/l_{12\%} = 1.764$ and $\tau_{4\%}/\tau_{12\%} = 1.453$ on average meaning the particles in 4% gel has about seventy-six percent longer walk length and forty-five percent longer sojourn time. Because the pore size of denser gel is smaller, the dye particles collide more frequently resulting in the walk length and sojourn time becoming shorter. We can make a similar analysis using υ and μ where $\upsilon_{4\%}/\upsilon_{12\%} = 1.214$ and $\mu_{4\%}/\mu_{12\%} = 0.688$ on average (Fig. S2). The first ratio implies that the mean speed υ of dye particles in the 4% acrylamide gel is about twenty-one percent faster than the other. The second ratio says the turning frequency (or collision frequency) μ is inversely proportional to the length scale of the acrylamide lattice and about thirty-one percent less. This further highlights that the dye particle collision with acrylamide structure is the deciding factor affecting the random walk environment of our system.

For comparison with other diffusion models (Fig. 4B, C): Chapman model gives, $l_{a\%}/l_{b\%} \sim$ const. and $\tau_{a\%}/\tau_{b\%} \sim R^{-2}$; Wereide's model gives $l_{a\%}/l_{b\%} \sim R$, and $\tau_{a\%}/\tau_{b\%} \sim$ const.; Fick model gives $l_{a\%}/l_{b\%} \sim R^2$ and $\tau_{a\%}/\tau_{b\%} \sim R^2$. Wereide and Chapman's models underestimate R dependency on random walk parameters, and Fick's model overestimates it. This agrees with our discussion above, where we mentioned that if $l(x)$ or $\tau(x)$ is constant or has the same dependence (i.e., $l(x)/\tau(x)$ is constant), the two-component diffusion model reduces into one of the single-component diffusion models. In other words, Wereide's model applies to systems where heterogeneity affects only the walk length, while Chapman's model applies to systems where heterogeneity affects only the sojourn time. Fick's model applies when both walk length and sojourn time have the same dependence on the system's heterogeneity, with the homogeneous system being the obvious case for it. Interestingly, this also indicates that there may be a system where D is position-dependent, but as long as $l(x)$ and $\tau(x)$ have the same position dependence, diffusion in such a system will follow Fick's model. Consistent with our expectation, we find the exponent corresponding to all of our experiments is $0 < q < 0.5$, and $l(x)$ and $\tau(x)$ depend on lattice size ratio R by the power of 3/2 and 1, respectively.

We initially hypothesized that $l_{4\%}/l_{12\%}$, the change in walk length from a 4% to a 12% gel, would be comparable to the change in lattice size R = 1.442, while the sojourn time remained largely unchanged. However, the fitted value for $l_{4\%}/l_{12\%}$ is 1.764. This difference may be explained by considering the effect of permeability on the walk length. For the acrylamide lattice of the lattice size L and the molecule size $r \sim 0.287$ nm, the permeability (p) is the area not obstructed by acrylamide divided by the lattice face area. Therefore, the permeability ratio between 4% and 12% gel is theoretically estimated to be $p_{4\%}/p_{12\%} = 1.184$. When the diffusion flux J for each gel percentage is multiplied by the corresponding permeability factor, this result is in line with the experimental permeability ratio $p_{4\%}/p_{12\%} = 1.223$ with $l_{4\%}/l_{12\%}$ reduced from 1.764 to 1.442, the same as R. Furthermore, the change in sojourn time $\tau_{4\%}/\tau_{12\%}$ decreases from 1.453 to 1.189 with the permeability considered.

CONCLUSION

We have investigated the fractionation of diffusing particles in a spatially controlled heterogeneous environment. The common intuition that random particle dispersal eventually homogenizes the distribution of particles holds true only in a homogeneous environment. Indeed, we have experimentally shown that the random dispersal of dye particles creates a fractionation phenomenon in a simple solid-solid interface of two types of acrylamide gels. This fractionation dynamics cannot be explained by conventional one-component diffusion models but are successfully described by the two-component diffusion model. The two components of the diffusion model can be expressed using random walk parameters such as the walk length l and the sojourn time τ. This model states that the equilibrium is achieved not when the mass density u is constant, but when $(l/\tau)u$ is constant. Since l/τ is the microscopic particle speed, we may say that the fractionation phenomenon is based on the fundamental physics principle that a steady state is achieved when the particle mass flux is balanced across the fractionation interface.

This paper highlights the nature of random dispersal in the presence of heterogeneity: fractionation is the macroscopic manifestation of the position-dependent coefficient $M(x)$, or equivalently, position-dependent random walk parameters such as walk length $l(x)$ and sojourn time $\tau(x)$. The Ludwig-Soret effect is one of the most well-known examples of fractionation, with over 160 years of history. A typical approach to explaining this phenomenon involves adding an advection term toward or against the temperature gradient ∇T. However, if diffusion coefficients depend on temperature (e.g., $M = M(T)$) and the temperature is spatially heterogeneous, then diffusion coefficients and random walk parameters become position-dependent. In such a case, the two-component diffusion flux produces a thermal advection term, which is $J_K = -K\nabla(Mu) = -D\nabla u - D\frac{M'(T)}{M(T)}u\nabla T$. Based on the observations in this paper, we conjecture that the thermal advection term also naturally arises from the two-component diffusion model and that no additional advection dynamics are present. We further conjecture that the exponent could be closer to $q = 1$ (Chapman's diffusion law) since the near incompressibility of liquid gives an almost uniform lattice size (i.e. $l(x)$ constant), but the temperature difference makes $\tau(x)$ vary as its internal energy increases with temperature, and it takes less time statistically between two jumps. The next step is to apply our system to a scenario similar to thermal diffusion phenomenon where dye particles are exposed to uniform lattice size (constant gel density) but with thermal gradient. This will involve quantitatively measuring and determining whether the two-component diffusion law alone can explain the thermal diffusion phenomenon.

MATERIALS AND METHODS

Polyacrylamide gels with heterogeneous lattice interface

Clear gel solutions are prepared by diluting Acrylamide/bis-acrylamide (37.5:1) 40% solution with triple distilled water to desired percentages (e.g., 12, 10, 5, and 4%). For colored gel solutions, two kinds of dyes are used in the experiment, Bromophenol Blue (BPB) and Rhodamine 6G (R6G). We have chosen them since they have long color fastness suitable for long observations. BPB samples are made by adding BPB to the diluted Acrylamide/Bis-acrylamide solution to the final dye concentration of 50 μg/ml. R6G samples are prepared similarly with the final dye concentration of 20 μg/ml.

We performed in total ten experiments, and each consists of four test subjects in gel casts: one heterogeneous gel combination, two homogeneous ones, and one reference one. The heterogeneous gel combination is assembled in gel cast. The gel cast is made of two parallel glass plates of dimensions 80 mm by 90 mm with a thin gap of 1 mm. Fresh 10% Ammonium Persulfate Solution (APS) and N,N,N',N'-Tetramethyl- ethylenediamine (TEMED) are added to BPB or R6G containing gel solution, which is then poured into the gel cast half full. To achieve a flat border between the types of gels, isopropyl alcohol is added on top and the gel is left to solidify. Then, we remove the isopropyl alcohol from the cast and rinse it several times with triple distilled water. The remaining half of the cast is filled with another colored gel with a different acrylamide percentage. The homogeneous gel combinations are assembled similarly but with the same acrylamide/bis-acrylamide percentage on both sides, with only one half with dye. Whether the colored gel is poured first or last affected the initial condition but did not matter in the measurement of homogeneous diffusivity. The reference gel combination is assembled by mixing the two gel solutions used in making the heterogeneous gel sample. The gel cast is filled with the mixture and polymerized as a whole. Once the gel solidified completely for each gel combination, the sample is sealed around the perimeter to inhibit the evaporation of solution from the gel.

Dye standard curve measurement

The standard curve for the dye molecules is measured to determine the optimal concentration of dye to be used during the experiment. A series of gels are made with increasing concentrations of BPB or R6G, and the absorbance of each gel is determined using a Luminograph. The range of dye concentration with linear correlation to the absorbance measured is selected as the optimal concentration.

Heterogeneous and homogeneous fractionation measurement

Diffusion measurements are performed over the sixty-four-hour period. We set the moment when the top part of the gel is poured as 0 hours. From then onwards, we took a photo of the test subject with the Luminograph at 1, 4, 9, 16, 25, 36, 49, and 64-hour marks, square of integers from one to eight, to observe the diffusion of dye particles. Since the diffusivity has the unit of m^2/s, measuring at these time intervals will yield uniform spatial step size. Samples are kept dark and moist to minimize exposure to light and prevent the gel from drying out.

Q_{frac} calculation

In order to quantify fractionation, we defined 'fractionation quotient' which measures the difference between the amount of dye on either side of the interface normalized by the initial net dye distribution at 4 hours. It is defined as $Q_{frac} = \frac{\left|\int_{\{x<0\}} u(t,x)\,dx - \int_{\{x>0\}} u(t,x)\,dx\right|}{\left|\int_{\{x<0\}} u_4(x)dx - \int_{\{x>0\}} u_4(x)dx\right|}$. This way, we were able to visualize the dynamics of fractionation over time, and compare different diffusion models.

Numerical methods

All simulations are performed in MATLAB using the 'pdepe' function, which is a built-in function that solves ordinary differential equations for each time step based on a variable-order, variable-step algorithm. The experimental data at 4hr are taken as initial data because the gel at 1hr is not yet hardened enough and requires extra time to be stabilized. The boundary condition is the no-flux boundary condition which is equivalent to the Neumann boundary condition. The domain of simulation is $-20 < x < 20$ which is the same as experimental dimension. (see SI: Parameter determination)

Global minimum of least square error

When we perform the numerical simulation, all parameters are obtained by the least square error. The least-square error between data and simulation is calculated at each time, from 9 hours to 64 hours. For all cases, one global minimum was obtained. It means that the experimental data are well explained by the diffusion equation and the unique minimizer can be used as the representative value for each parameter.

Numerical estimation for homogeneous diffusion

First, the diffusivity of each concentration is measured from two homogeneous gels respectively. To simulate the diffusion phenomena, the homogeneous diffusion equation is used which is $u_t = D_{a\%}\, u_{xx}$, where $D_{a\%}$ denotes the diffusivity of BPB dye in the a% polyacrylamide gel. It is attained by minimizing the least square error. The snapshots of both experiment data and numerical simulation have a single intersection point at the middle of each front. This is a special feature of diffusion phenomena and indicates that the experiment is represented well by the diffusion equation.

Numerical estimation for heterogeneous diffusion

Similarly, the heterogeneous diffusion equation used in the numerical estimation is $u_t = [K(x)(M(x)u)_x]_x = [D^{1-q}(x)(D^q(x)u)_x]_x$, where the exponent q is a control variable. For single component diffusion models, q values of 0, 0.5 and 1 were used for Fick, Wereide and Chapman respectively. For our two-component diffusion model, the optimal q is attained by minimizing the least square error between data and simulation for each experiment group. For $D(x)$, although we assume jump discontinuity of the diffusivity at $x = 0$, there is an intermediate region between the acrylamide gels, where it smoothly connects the two regions. Due to this transition layer at the interface, we use an approximation technique. Thus, the diffusivity used in the simulation is an inverse tangent function, more precisely $D(x) = A + B\, arctan(3x)$ to account for the continuous transition layer. Among the domain $-20 < x < 20$, the *arctan* function can recover 89.51% of the jump discontinuity at $-2 < x < 2$. This $D(x)$, combined with the initial experimental data at 4 hours, is used to numerically estimate fractionation for both single component diffusion models (Fick, Wereide, and Chapman) and our two-component diffusion model.

Data extraction process from raw data

Step 1. The pictures of gel samples are taken by a Luminograph as raw data (SI raw data 1~10: Interdiffusion row shows the heterogeneous experiment). Step 2. To remove the refraction effect of the lens, a background image is used, and the light intensity of each pixel is obtained by subtracting the background intensity from the data intensity. After that, we arrange all images by rigid rotation, using 'imregister' function in MATLAB. Step 3. From the obtained light intensity, 600 × 500 pixels are chosen near the middle of the images. To remove noise, 'trimmean' function in MATLAB is used as a smoothing function. Step 4. Take the average value of each row. Then, a vector of 600 components of the light intensity is obtained, and each element represents 1/300 inch (or 300 dpi). Step 5. To convert the light intensity to concentration, we need to follow the following three processes: 1) The average light intensity of each image and the maximal intensity of reference gel are used to determine the standard curve between light intensity and transmittance. 2) Using the relationship between transmittance and absorbance, the absorbance vector is obtained. 3) Using Beer-Lambert law, the light intensity vector is transformed to the concentration vector. Putting all steps together, the relation between light intensity and concentration is Concentration = 50 μg/mL × $\frac{\log \mathrm{M} - \log(\text{Light intensity})}{\log \mathrm{M} - \log \mathrm{A}}$ where M is the maximum light intensity and A is the average light intensity. Then, 600 components vector of concentration is obtained, and it is compared with the simulation in the following steps. Step 6. From homogeneous gel, perform a simulation with the initial value equal

to 4 hours data. The diffusivity $D_{a\%}$ is a manipulated variable and it is determined by minimizing the least square error. Step 7. From heterogeneous gel, perform a simulation with the initial value equal to 4 hours data. Since the diffusivity is determined in the previous step, the only manipulated variable is q. It is also determined by minimizing the least square error.

AUTHOR INFORMATION

Corresponding Authors

Myung Chul Choi - Department of Bio and Brain Engineering, Korea Advanced Institute of Science and Technology (KAIST), Daejeon 34141, Republic of Korea; orcid.org/0000-0003-3811-5279; E-mail: mcchoi@kaist.ac.kr

Yong-Jung Kim - Department of Mathematical Science, Korea Advanced Institute of Science and Technology (KAIST), Daejeon 34141, Republic of Korea; orcid.org/0000-0003-0968-4093; E-mail: yongkim@kaist.ac.kr

Authors

Hoyoun Kim - *Department of Mathematical Science, Korea Advanced Institute of Science and Technology (KAIST), Daejeon 34141, Republic of Korea*; orcid.org/0000-0003-1606-2671; E-mail: ghsl0615@gmail.com

KeunMin Ken Lee - *Department of Bio and Brain Engineering, Korea Advanced Institute of Science and Technology (KAIST), Daejeon 34141, Republic of Korea*; orcid.org/0009-0003-2180-7575; E-mail: thermsals@gmail.com

Gadisa Firisa - *Department of Bio and Brain Engineering, Korea Advanced Institute of Science and Technology (KAIST), Daejeon 34141, Republic of Korea*; E-mail: gaaddisaa@kaist.ac.kr

Juncheol Lee - *Department of Bio and Brain Engineering, Korea Advanced Institute of Science and Technology (KAIST), Daejeon 34141, Republic of Korea*; orcid.org/0000-0002-7218-2072; E-mail: ljc0626@gmail.com

Present Addresses

[§]**Hoyoun Kim** - Computer, Electrical and Mathematical Sciences and Engineering Division (CEMSE), King Abdullah University of Science and Technology (KAUST); Thuwal, 23955, the Kingdom of Saudi Arabia.

Author Contributions

[#]Hoyoun Kim and KeunMin Ken Lee contributed equally.

Acknowledgement

This work was supported by NRF-2020M3A7B6026565, RS-2024-00347311, RS-202300277142, RS-2023-KH135534, RS-2024-00354741, KC30-N11230021, KBSI-2021R1A6C103B422. H.K. is partially supported by King Abdullah University of Science and Technology baseline funds.

REFERENCES

(1) Einstein, A. On the Movement of Small Particles Suspended in a Stationary Liquid Demanded by the Molecular-Kinetic Theory of Heat. *Ann. Phys.* **1905**, *322* (8), 549–560.

(2) Ludwig, C. Diffusion Zwischen Ungleich Erwärmten Orten Gleich Zusammengesetzter Lösungen. *Sitzungsber Akad Wiss Wien Math-Naturwiss* **1856**, *20*, 539.

(3) Soret, C. Sur l'état d'équilibre Que Prend Au Point de Vue de Sa Concentration Une

Dissolution Saline Primitivement Homogène Dont Deux Parties Sont Portées à Des Températures Différentes. *Arch. Sci. Phys. Nat* **1879**, *2*, 48–61.

(4) Leng, J.; Guo, Z.; Zhang, H.; Chang, T.; Guo, X.; Gao, H. Negative Thermophoresis in Concentric Carbon Nanotube Nanodevices. *Nano Lett.* **2016**, *16* (10), 6396–6402. https://doi.org/10.1021/acs.nanolett.6b02815.

(5) A. E. Schoen, P.; H. Walther, J.; Arcidiacono, S.; Poulikakos, D.; Koumoutsakos, P. Nanoparticle Traffic on Helical Tracks: Thermophoretic Mass Transport through Carbon Nanotubes. *Nano Lett.* **2006**, *6* (9), 1910–1917. https://doi.org/10.1021/nl060982r.

(6) Barreiro, A.; Rurali, R.; Hernández, E. R.; Moser, J.; Pichler, T.; Forró, L.; Bachtold, A. Subnanometer Motion of Cargoes Driven by Thermal Gradients Along Carbon Nanotubes. *Science (80-.).* **2008**, *320* (5877), 775–778. https://doi.org/10.1126/science.1155559.

(7) Keith, C. H.; Derrick, J. C. Measurement of the Particle Size Distribution and Concentration of Cigarette Smoke by the "Conifuge." *J. Colloid Sci.* **1960**, *15* (4), 340–356. https://doi.org/https://doi.org/10.1016/0095-8522(60)90037-4.

(8) Jennings, S. G. The Mean Free Path in Air. *J. Aerosol Sci.* **1988**, *19* (2), 159–166. https://doi.org/https://doi.org/10.1016/0021-8502(88)90219-4.

(9) Elliott, G. A.; Masson, I. Thermal Separation in Gaseous Mixtures. *Proc. R. Soc. London. Ser. A, Contain. Pap. a Math. Phys. Character* **1925**, *108* (746), 378–385.

(10) Dominguez, G.; Wilkins, G.; Thiemens, M. H. The Soret Effect and Isotopic Fractionation in High-Temperature Silicate Melts. *Nat. 2011 4737345* **2011**, *473* (7345), 70–73. https://doi.org/10.1038/nature09911.

(11) Darken, L. S. Diffusion of Carbon in Austenite with a Discontinuity in Composition. *Philadelphia Meeting*. 1948, pp 430–438. https://cir.nii.ac.jp/crid/1572824499500645504 (accessed 2023-03-02).

(12) Skaug, M. J.; Mabry, J.; Schwartz, D. K. Intermittent Molecular Hopping at the Solid-Liquid Interface. *Phys. Rev. Lett.* **2013**, *110* (25), 256101. https://doi.org/10.1103/PhysRevLett.110.256101.

(13) León-Cázares, F. D.; Galindo-Nava, E. I. General Model for the Kinetics of Solute Diffusion at Solid-Solid Interfaces. *Phys. Rev. Mater.* **2021**, *5* (12), 123802. https://doi.org/10.1103/PHYSREVMATERIALS.5.123802/FIGURES/13/MEDIUM.

(14) Nernst, W. Zur Kinetik Der in Lösung Befindlichen Körper. *Zeitschrift für Phys. Chemie* **1888**, *2U* (1), 613–637. https://doi.org/10.1515/ZPCH-1888-0274.

(15) Van Milligen, B. P.; Bons, P. D.; Carreras, B. A.; Śnchez, R. On the Applicability of Fick's Law to Diffusion in Inhomogeneous Systems. *Eur. J. Phys.* **2005**, *26* (5), 913–925. https://doi.org/10.1088/0143-0807/26/5/023.

(16) Brangwynne, C. P.; Tompa, P.; Pappu, R. V. Polymer Physics of Intracellular Phase Transitions. *Nat. Phys.* **2015**, *11* (11), 899–904. https://doi.org/10.1038/nphys3532.

(17) Ahmed, T.; Zhang, Y.; Lee, J. H.; Styczynski, M. P.; Takayama, S. Nucleic Acid Partitioning in PEG-Ficoll Protocells. *J. Chem. Eng. Data* **2022**, *67* (8), 1964–1971. https://doi.org/10.1021/acs.jced.2c00042.

(18) Savastano, A.; Flores, D.; Kadavath, H.; Biernat, J.; Mandelkow, E.; Zweckstetter, M. Disease-Associated Tau Phosphorylation Hinders Tubulin Assembly within Tau Condensates. *Angew. Chemie - Int. Ed.* **2021**, *60* (2), 726–730. https://doi.org/10.1002/anie.202011157.

(19) Kim, H.; Ling, S. C.; Rogers, G. C.; Kural, C.; Selvin, P. R.; Rogers, S. L.; Gelfand, V. I. Microtubule Binding by Dynactin Is Required for Microtubule Organization but Not Cargo Transport. *J. Cell Biol.* **2007**, *176* (5), 641–651. https://doi.org/10.1083/jcb.200608128.

(20) Rivolta, I.; Panariti, A.; Collini, M.; Lettiero, B.; D'Alfonso, L.; Sironi, L.; Miserocchi, G.; Chirico, G. A Biophysical Model of Intracellular Distribution and Perinuclear Accumulation of Particulate Matter. *Biophys. Chem.* **2011**, *158* (2–3), 134–140.

https://doi.org/10.1016/j.bpc.2011.06.009.
(21) K. Chakraborty, S.; A. J. Fitzpatrick, J.; A. Phillippi, J.; Andreko, S.; S. Waggoner, A.; P. Bruchez, M.; Ballou, B. Cholera Toxin B Conjugated Quantum Dots for Live Cell Labeling. *Nano Lett.* **2007**, *7* (9), 2618–2626. https://doi.org/10.1021/nl0709930.
(22) Wei, W.; Ma, G.-H.; Hu, G.; Yu, D.; Mcleish, T.; Su, Z.-G.; Shen, Z.-Y. Preparation of Hierarchical Hollow CaCO3 Particles and the Application as Anticancer Drug Carrier. *J. Am. Chem. Soc.* **2008**, *130* (47), 15808–15810. https://doi.org/10.1021/ja8039585.
(23) Chapman, S. On the Partial Separation by Thermal Diffusion of Gases of Equal Molecular Weight. *London, Edinburgh, Dublin Philos. Mag. J. Sci.* **1917**, *34* (200), 146–151.
(24) Chapman, S. On the Brownian Displacements and Thermal Diffusion of Grains Suspended in a Non-Uniform Fluid. *Proc. R. Soc. London. Ser. A, Contain. Pap. a Math. Phys. Character* **1928**, *119* (781), 34–54. https://doi.org/10.1098/rspa.1928.0082.
(25) D.Sc., S. C. M. A.; Sc.D., F. W. D. M. A. XXII. A Note on Thermal Diffusion. *London, Edinburgh, Dublin Philos. Mag. J. Sci.* **1917**, *33* (195), 248–253. https://doi.org/10.1080/14786440308635635.
(26) Chapman, S.; Cowling, T. *The Mathematical Theory of Non-Uniform Gases.*, 3rd ed.; Cambridge University Press, 1970. https://doi.org/10.2307/3609795.
(27) Enskog, D. Kinetische Theorie Der Vorgänge in Mässig Verdünnten Gasen.; Ph.D. Dissertation, Lund University, Lund, Sweden, 1917.
(28) Wereide, M. T. La Diffusion d'une Solution Dont La Concentration et La Température Sont Variables. *Ann. Phys. (Paris).* **1914**, *9* (2), 67–83. https://doi.org/10.1051/anphys/191409020067.
(29) Furry, W. H.; Jones, R. C.; Onsager, L. On the Theory of Isotope Separation by Thermal Diffusion. *Phys. Rev.* **1939**, *55* (11), 1083–1095. https://doi.org/10.1103/PhysRev.55.1083.
(30) Artola, P. A.; Rousseau, B.; Galliéro, G. A New Model for Thermal Diffusion: Kinetic Approach. *J. Am. Chem. Soc.* **2008**, *130* (33), 10963–10969. https://doi.org/10.1021/ja800817f.
(31) Duhr, S.; Braun, D. Why Molecules Move along a Temperature Gradient. *Proc. Natl. Acad. Sci. U. S. A.* **2006**, *103* (52), 19678–19682. https://doi.org/10.1073/pnas.0603873103.
(32) Van Kampen, N. G. Diffusion in Inhomogeneous Media. *J. Phys. Chem. Solids* **1988**, *49* (6), 673–677. https://doi.org/10.1016/0022-3697(88)90199-0.
(33) Schnitzer, M. J. Theory of Continuum Random Walks and Application to Chemotaxis. *Phys. Rev. E* **1993**, *48* (4), 2553. https://doi.org/10.1103/PhysRevE.48.2553.
(34) Landsberg, P. T. D Grad ν or Grad(Dν)? *J. Appl. Phys.* **1998**, *56* (4), 1119. https://doi.org/10.1063/1.334083.
(35) Sattin, F. Fick's Law and Fokker–Planck Equation in Inhomogeneous Environments. *Phys. Lett. A* **2008**, *372* (22), 3941–3945. https://doi.org/10.1016/J.PHYSLETA.2008.03.014.
(36) Kim, Y.-J. Einstein's Random Walk and Thermal Diffusion. *arXiv* **2013**. https://doi.org/10.48550/arxiv.1307.4460. (accessed 2023-03-03)
(37) Cho, E.; Kim, Y. J. Starvation Driven Diffusion as a Survival Strategy of Biological Organisms. *Bull. Math. Biol.* **2013**, *75* (5), 845–870. https://doi.org/10.1007/S11538-013-9838-1/FIGURES/8.
(38) Kim, H. Y.; Kim, Y. J.; Lim, H. J. Heterogeneous Discrete Kinetic Model And Its Diffusion Limit. *Kinet. Relat. Model.* **2021**, *14* (5), 749–765. https://doi.org/10.3934/krm.2021023.
(39) Kim, Y. J.; Seo, H. Model for Heterogeneous Diffusion. *SIAM J. Appl. Math.* **2021**, *81* (2), 335–354. https://doi.org/10.1137/19M130087X.
(40) Lim, H.-J.; Kim, Y.-J. Heterogeneous Discrete-Time Random Walk and Reference Point Dependency. *Preprint* **2023**.
(41) Holmes, D. L.; Stellwagen, N. C. Estimation of Polyacrylamide Gel Pore Size from Ferguson

Plots of Normal and Anomalously Migrating DNA Fragments. I. Gels Containing 3 % N, N′-Methylenebisacrylamide. *Electrophoresis* **1991**, *12* (4), 253–263. https://doi.org/10.1002/ELPS.1150120405.

(42) Chapman, S. On the Brownian Displacements and Thermal Diffusion of Grains Suspended in a Non-Uniform Fluid. *Proc. R. Soc. London. Ser. A, Contain. Pap. a Math. Phys. Character* **1928**, *119* (781), 34–54. https://doi.org/10.1098/rspa.1928.0082.

TOC Graphic

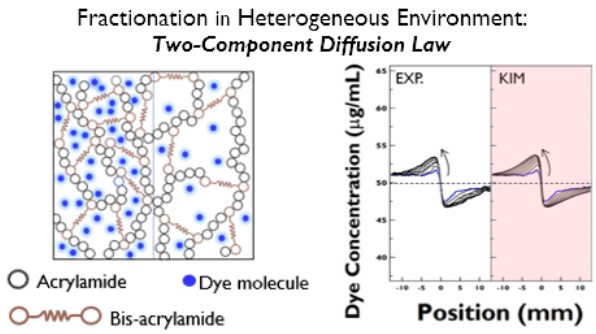
Fractionation in Heterogeneous Environment:
Two-Component Diffusion Law
Acrylamide
Dye molecule
Bis-acrylamide
EXP.
KIM
Dye Concentration (μg/mL)
Position (mm)